Preferred formation of heteromeric channels between co-expressed SK1 and IKCa channel subunits provides a unique pharmacological profile of Ca^{2+}-activated potassium channels

James Higham*, Giriraj Sahu[+], Rima-Marie Wazen[‡], Pina Colarusso[‡], Alice Gregorie*, Bartholomew S. J. Harvey*, Lucy Goudswaard*, Gemma Varley*, David N. Sheppard*, Ray W. Turner[+], Neil V. Marrion*[1]

*School of Physiology, Pharmacology & Neuroscience, University of Bristol, Bristol, BS8 1TD, UK.

[+]Hotchkiss Brain Institute, [‡]Snyder Institute for Chronic Diseases, Cumming School of Medicine, University of Calgary, Calgary, Alberta, Canada T2N 4N1

Running title: Co-assembly of SK1 and IKCa subunits

[1]Author for correspondence: Prof. N.V. Marrion, School of Physiology, Pharmacology & Neuroscience, Faculty of Life Sciences, University of Bristol, Bristol, BS8 1TD.

Email: N.V.Marrion@bristol.ac.uk

Tel: +441173311401

Non-standard abbreviations:

SK – small conductance calcium-activated potassium channel

IKCa – intermediate conductance calcium-activated potassium channel

STORM – Stochastic Optical Reconstruction Microscopy

FRET- Fluorescence Resonance Energy Transfer

UCL1684 - 6,12,19,20,25,26-Hexahydro-5,27:13,18:21,24-trietheno-11,7-metheno-7*H*-dibenzo [*b*,*n*] [1,5,12,16]tetraazacyclotricosine-5,13-diium dibromide

Ctx - charbydotoxin

TRAM-34 - 1-[(2-Chlorophenyl)diphenylmethyl]-1*H*-pyrazole

DMSO – Dimethyl sulfoxide

IC_{50} – inhibitory concentration 50

Abstract

Three SK channel subunits have been cloned and found to preferentially form heteromeric channels when expressed in a heterologous expression system. The original cloning of the gene encoding the IKCa channel was termed SK4, because of the high homology between channel subtypes. Recent immunovisualization suggests that IKCa is expressed in the same subcellular compartments of some neurons as SK channel subunits. STORM super-resolution microscopy revealed that co-expressed IKCa and SK1 channel subunits were closely associated, a finding substantiated by measurement of FRET between co-expressed fluorophore-tagged subunits. Expression of homomeric SK1 channels produced current that displayed typical sensitivity to SK channel inhibitors, while expressed IKCa channel current was inhibited by known IKCa channel blockers. Expression of both SK1 and IKCa subunits gave a current that displayed no sensitivity to SK channel inhibitors and a decreased sensitivity to IKCa current inhibitors. Single channel recording indicated that co-expression of SK1 and IKCa subunits produced channels with properties intermediate between those observed for homomeric channels. These data indicate that SK1 and IKCa channel subunits preferentially combine to form heteromeric channels that display pharmacological and biophysical properties distinct from those seen with homomeric channels.

Introduction

The cloning of SK channels identified 3 channel subtypes, termed SK1-3, which are widely expressed in various tissues (Weatherall *et al.*, 2010). For example, activation of these channels by a rise of intracellular calcium (Ca^{2+}) underlies generation of the medium afterhyperpolarization in hippocampal neurons (Stocker *et al.*, 1999; Bond *et al.*, 2004). In contrast, cloning of the cDNA encoding IKCa channels found a sequence that showed approximately 40% similarity at the amino acid level with SK channels (Joiner *et al.*, 1997). This level of homology ensured that the clone was originally named SK4. This subunit was originally identified in epithelial- and

endothelial-rich tissues and in the immune system (Balut *et al.*, 2012). Expression of IKCa subunits gave rise to Ca^{2+}-activated channels that like SK1-3 channels, produced a voltage-independent current (Joiner *et al.*, 1997). However, the pharmacology of SK4-mediated current is very different from SK1-3-mediated current and expressed SK4 channels exhibit a higher single channel conductance than expressed SK channels (Kohler *et al.*, 1996; Joiner *et al.*, 1997).

Co-expression of SK channel subtypes has been demonstrated to form heteromeric channels (Church *et al.*, 2015; Hancock *et al.*, 2015). It is particularly obvious with co-expression of SK1 and SK2 subunits that heteromeric channels are preferentially formed, giving rise to a heteromeric channel that exhibits a sensitivity to inhibition by apamin that is intermediate to that observed with homomeric channels (Church *et al.*, 2015). SK channel subunits co-assemble by interaction between the carboxyl termini of subunits to form functional channels. The degree of amino acid sequence homology between carboxyl termini of IKCa and SK channels suggests that heteromerization might occur. It has been recently shown that IKCa subunit expression also occurs in the same cell types as SK channel subunits. IKCa subunits are expressed in neurons (Neylon *et al.*, 2004; Mongan *et al.*, 2005; Nguyen *et al.*, 2007; Engbers *et al.*, 2012; King *et al.*, 2015; Turner *et al.*, 2015, 2016) with for example, IKCa subunits being expressed with all SK channel subunits in dorsal root ganglion and spinal cord neurons (Mongan *et al.*, 2005). In addition, IKCa subunits are expressed in brain regions, such as cortex, cerebellum and thalamus (Mongan *et al.*, 2005; Engbers *et al.*, 2012; Turner *et al.*, 2015, 2016). In particular, IKCa subunits are expressed in the soma of hippocampal neurons, coincident with the location of expressed SK1 subunits (Bowden *et al.*, 2001; Turner *et al.*, 2015, 2016).

We find through Stochastic Optical Reconstruction Microscopy (STORM) imaging and Fluorescence Resonance Energy Transfer (FRET) that IKCa and SK1 fluorescent signals are closely associated when co-expressed in tsA-201 cells. Super-resolution imaging revealed overlapping clusters of fluorescent labels of tagged channels, and the strict requirements for

proximity of proteins to exhibit FRET are consistent with the formation of heteromeric channels by IKCa and SK1 subunits. Expression of homomeric SK1 or IKCa channels gave currents that were sensitive to classical inhibitors/blockers, whilst co-expression of both subunits formed heteromeric channels with distinct pharmacology. Single-channel analysis showed that co-expression of both subunits formed heteromeric channels with properties that were intermediate between those exhibited by each homomeric channel. These data demonstrate that IKCa and SK1 subunits prefer to form heteromeric channels when co-expressed in a heterologous system that will alter their responsiveness to pharmacological tools typically used to define their expression pattern.

Methods

Direct Stochastic Optical Reconstruction Microscopy (STORM):

Immunostaining:

For STORM imaging tsA-201 cells grown on 18 mm No 1.5 coverslips (VWR VistaVision, Canada) at 37 ºC were transfected with untagged human SK1 (hSK1) and human IKCa (hIKCa) cDNAs. After 32-48 hours cells were washed with 1X PBS (Sigma Aldrich, Canada) followed by fixation in 4% paraformaldehyde (Electron Microscopy Sciences, Canada) in 1X PBS for 10 min. After 3 rounds of washing in 1X PBS, cells were incubated with blocking medium consisting of 1X PBS, 5% (w/v) bovine serum albumin and 0.2% (v/v) Triton X-100 for 45 min at room temperature (RT) (~25 ºC). Cells were then incubated in blocking solution containing primary antibodies against SK1 (rabbit anti-KCa2.1; APC-039, Alomone Labs, Israel) and IKCa channels (mouse monoclonal IK1; sc-365265, Santa Cruz Biotechnology, USA) at 1:250 dilution for 45 min (RT). After washing three times with blocking medium for 10 min each (RT), cells were treated with Alexa Fluor-647 conjugated goat $F(ab')_2$ anti-rabbit IgG (111-606-047, Jackson ImmunoResearch, USA) or Cy-3 conjugated rabbit $F(ab')_2$ anti-mouse IgG (315-166-047, Jackson ImmunoResearch, USA) in blocking medium at 1:1000 dilution for 45 min (RT). Stained cells were post fixed in 4%

paraformaldehyde and 0.1% glutaraldehyde solution in 1X PBS for 10 min. TetraSpek™ beads (100 nm diameter, Thermo Fisher) were added to the coverslips for 30 min (RT) and then cells were thoroughly washed and stored at 4 ºC in 1X PBS until imaging. The specificity of anti-hSK1 and anti-hIKCa antibodies was verified by co-labelling tsA-201 cells expressing either cDNA in isolation (Supplemental Figure 1). Labeling and imaging was performed from cells prepared from a minimum of 3 different experiments.

dSTORM data acquisition:

STORM imaging was performed in a freshly prepared buffer consisting of 1X PBS, 10% (w/v) glucose, 10 mM β-mercaptoethanol as well as an oxygen-scavenging GLOX solution containing 0.5 mg/ml glucose oxidase (Sigma-Aldrich) and 40 µg/ml catalase (Sigma-Aldrich). 10X GLOX solution was prepared as a stock and stored in aliquots at -20 ºC. On the day of imaging, one aliquot of GLOX solution was thawed and used to prepare the dSTORM imaging buffer. Cells on 18 mm coverslips were then sealed onto concavity slides (Eisco Labs, Canada) containing STORM imaging buffer with the help of VALAP sealing (equal parts of paraffin, Vaseline, and lanolin).

Samples were positioned on the piezo Z-controlled stage of a Diskovery Flex microscope (Quorum Technologies, Guelph, ON, Canada) equipped with 405, 561 and 637 nm solid-state laser lines. TIRF illumination was employed using using a Leica HC Plan Apo 63X/NA 1.47 oil immersion objective, and the stochastic blinking was detected with an Andor iXon Ultra 897 EMCCD camera. TIRF signal was imaged within 100-150 nm of the membrane surface. Stronger intensity laser illumination was used to photoswitch the vast majority of fluorophores into a temporary dark state (laser power: 561 nm, 55 mW @ 100%; 647 nm, 53 mW @ 100%). Subsets of active fluorophores were then imaged at a lower laser intensity (70-95% excitation) at 20 ms intervals (frame rate of 50 Hz) between consecutive frames. During image acquisition, the 405 nm laser line was used to re-activate the Alexa Fluor-647 or Cy-3 dyes. For individual

experiments 20,000 to 35,000 image frames were acquired that were further processed offline to reconstruct a super-resolution image.

Image reconstruction and analysis:

Image reconstruction of the STORM data streams was carried out using the ThunderSTORM plug-in for FIJI (ImageJ) (Schindelin *et al.*, 2012; Ovesny *et al.*, 2014). Using this plug-in, the image streams were wavelet filtered using defined camera settings (Pixel size: 150 nm; photoelectrons per A/D count: 8.98; base level A/D count: 200; EM gain: 300) and rendered as a 2D Gaussian fit of each localization. Single molecule events were detected using an 8-point neighbourhood local maxima principle and a weighted least square fitting of 2D Gaussian used to localize the sub-pixel centroids. The reconstructed images were displayed using a normalized Gaussian algorithm. Cross correlation and fiducial bead-based drift correction was carried out through alignment of 3-6 100 nm fiducial TetraSpek™ beads (Thermo Fisher, Canada) contained within the field of view to ensure the images were registered spatially. In most cases, mechanical drift over the timeframe required for imaging (30-40 min) ranged no more than 0-500 nm, with any cases approaching 1 µm excluded from analysis. Spatial coordinates (X and Y) and intensity information of individual point localizations were exported as a text file for further analysis in the open source Localization Microscopy Analyzer software (LAMA) (Malkusch and Heilemann, 2016) and in MATLAB. The X-Y coordinates of fiducial beads were used as the reference point to align signals for IKCa and hSK1 channels using the affain registration function of LAMA.

Cluster analysis:

Clusters of individual proteins were detected based upon size and intensity information employing a morphological cluster analysis algorithm (LAMA) (Malkusch and Heilemann, 2016). The background intensity level was used for thresholding the data sets. A minimum radius criterion of 40 nM was set for cluster detection considering that localization precision was ~25-35 nm, excluding from analysis clusters less than 40 nm diameter. The cluster centroid (X, Y) positions

outputted by LAMA were calculated to determine the distances between clusters of fluorophores tagged to hSK1 or IKCa channels, and between the clusters of tagged hSK1 and IKCa channels using Matlab. In all, the minimum Euclidean distances between the points in the hSK1 data sets, the IKCa data sets, and between the hSK1 and IKCa data sets were determined. Cluster sizes are presented as mean ± SD across 7 cells by STORM imaging of ~450-1000 clusters per cell. Mean values presented were thus derived from 3866 clusters of hIKCa and 3059 clusters of hSK1 immunolabels. The sample value (n=7) thus represents the number of cells from which all clusters were identified.

Fluorescence Resonance Energy Transfer (FRET):

For FRET imaging, tsA-201 cells were seeded onto poly-L-lysine coated 35 mm glass bottom petri dishes. Fluorescent tagged constructs were generated using PCR based amplification of hSK1 and hIKCa open reading frames, excluding the stop codon, bearing overhanging HindIII and AgeI restriction sites. Amplified products of hSK1 and hIKCa and empty pmKate2 vector were double digested with HindIII and AgeI restriction enzymes (NEB, USA) followed by ligation with T4 DNA ligase (NEB, USA) for generation of hSK1-eGFP and hIKCa-mKate (pmKate2 referred to as mKate throughout) tagged constructs. In both hSK1-eGFP and hIKCa-mKate, fluorophores were attached to the C-terminus of hSK1 and hIKCa channels. Restriction digestion and DNA sequencing was carried out to validate tagged constructs.

For FRET analysis, cells were transiently transfected with combinations of hSK1-eGFP (2 µg/ml cDNA), hIKCa-mKate (2 µg/ml cDNA), eGFP (2 µg/ml cDNA) or mKate (2 µg/ml cDNA). Cells were then incubated for 48 h at 37 °C and 5% CO_2, washed and replaced with colorless imaging medium comprised of 148 mM NaCl, 3 mM KCl, 10 mM HEPES, 3 mM $CaCl_2$, 10 mM glucose, 1 mM $MgCl_2$, pH 7.3 at 25 °C. Cells were examined with a Nikon C1si spectral confocal laser-scanning microscope with a 40x/1.3NA oil immersion objective. hSK1-eGFP was excited at 457 nm and hIKCa-mKate at 561 nm. Emission spectra of eGFP and mKate were recorded between

400 - 750 nm and ImageTrak software (P.K. Stys, http://www.ucalgary.ca/styslab/imagetrak) used to analyze the imaging data as previously (Asmara *et al.*, 2017; Sahu *et al.*, 2017). Spectral images were linearly unmixed, collapsing a 32-channel spectral image into a 2-channel image representing the integrated intensities of eGFP and mKate fluorescence emissions. Efficiency of FRET energy transfer was calculated using the formula: $E_{FRET} = F_A/(F_A + F_D)$, where F_A corresponds to peak emission intensity of acceptor fluorophore, F_D corresponds to peak emission intensity value of donor fluorophore, and E_{FRET} corresponds to efficiency of FRET between donor and acceptor fluorophore (Erkens et al., 2013).

Cell culture and electrophysiology:

The tsA201 cell line was maintained as described previously (Lamy *et al.*, 2010). Cells were transiently transfected with hSK1 or hIKCa or both using polyethyleneimine (Alfa Aesar, Inc.) by combining channel plasmid DNA with enhanced green fluorescent protein (eGFP) cDNA in a ratio of 1:5 (maximal plasmid content: 1.5 µg). The ratio of co-expressed subunit plasmid DNA was 1:1. Cells were used for electrophysiology 16-24 h after transfection. For functional validation of the hSK1-eGFP and hIKCa-mKate cDNAs used for FRET imaging 2 µg of either cDNAs was co-transfected with eGFP (1 µg/ml) in tsA-201 cells using a calcium-phosphate based transfection reagent and whole-cell patch-clamp recordings performed 24-48 h after transfection.

Electrophysiology: Expressed currents were recorded in the excised outside-out patch configuration for pharmacology, and in the whole-cell configuration to verify tagged construct properties using symmetrical high (~160 mM) K^+ conditions and an internal solution that contained 1 µM free Ca^{2+}. Pipettes were fabricated from KG-33 glass (Friedrich & Dimmock, Inc.) and filled with an internal solution of composition: KAsp (97 mM) and KCl (20 mM) or KCl (117 mM), HEPES (10 mM), EGTA (10 mM), Na_2ATP (1.5 mM), $CaCl_2$ (9.65 mM, calculated free $[Ca^{2+}]_i$ 1 µM), $MgCl_2$ (2.34 mM, calculated free $[Mg^{2+}]_i$ 1 mM), pH 7.4, with ~40 mM KOH. Cells were bathed in a control external solution that consisted of: KAsp (97 mM) and KCl (20 mM) or KCl (127 mM),

HEPES (10 mM), EGTA (10 mM), $CaCl_2$ (6.19 mM, calculated free $[Ca^{2+}]_i$ 60 nM), $MgCl_2$ (1.44 mM, calculated free $[Mg^{2+}]_i$ 1 mM), pH 7.4, with ~40 mM KOH. Expressed currents were revealed by a 1 s voltage ramp from -100 to +100 mV. Apamin (Sigma Aldrich, UK or Abcam, Canada), 6,12,19,20,25,26-Hexahydro-5,27:13,18:21,24-trietheno-11,7-metheno-7*H*-dibenzo[*b*,*n*] [1,5,12,16] tetraazacyclotricosine-5,13-diium dibromide (UCL1684;Tocris Biosciences, Bristol, UK), charybdotoxin (Ctx; Santa Cruz Biotechnology, USA) and 1-[(2-Chlorophenyl)diphenylmethyl]-1*H*-pyrazole (TRAM-34; Tocris Biosciences, UK / Canada) were added to external bath solution. TRAM-34 was dissolved in DMSO at 10 mM stock concentration and aliquots stored at -20 °C until used. UCL1684 was dissolved at a stock concentration of 100 µM in DMSO and aliquots stored at -20 °C. Finally, apamin and Ctx were dissolved in distilled water at a stock concentration of 100 µM and aliquots stored at -20 °C. All compounds were defrosted on the day of recording, with aliquots only thawed once, and desired concentrations prepared by dilution in bath solution.

For concentration-inhibition relationships, data points representing current block were fit with a variable slope Hill equation in the form:

$$I \,/\, I_{cont} = A_{min} + \left(\frac{A_{max} - A_{min}}{1 + 10^{(LogIC_{50} - X) \times n_h}}\right)$$

where I_{cont} is the amplitude of current at -60 mV in the absence of drug, I is the amplitude of current observed at a given concentration of blocker ([*X*], expressed in logarithmic units), A_{min} is I_{min}/I_{cont}, A_{max} is I_{max}/I_{cont}, IC_{50} is the concentration of blocker that blocks 50% of the sensitive current, and n_h is the Hill coefficient.

Inside-out patch electrophysiology

HEK293 cells expressing hSK1, hIKCa, or hSK1 and hSK1 channel subunits were bathed in a solution of composition (mM): : KAsp (97 mM), KCl (30 mM), HEPESNa (10 mM), EGTA (10 mM), $CaCl_2$ (9.28 mM, calculated free $[Ca^{2+}]_i$ 1 µM), $MgCl_2$ (2.5 mM, calculated free $[Mg^{2+}]_i$ 1 mM), pH 7.4, with ~40 mM KOH. Quartz electrodes (1.5 mm OD, 0.5 mm ID) quartz electrodes were filled with the same solution and had resistances of 8-14 MΩ. Channel activity was recorded at -30, -

50, -70 and -90 mV from a holding potential of 0 mV, with all potentials expressed as the negative of that which was applied to the patch. Data were acquired with an Axopatch 200A amplifier, filtered at 1 kHz (low-pass 8-pole Bessel) and sampled at 10 kHz using Pulse (HEKA, Germany). Single channel events were analysed using Tac and TacFit (Bruxton, USA) which utilises a spline interpolation procedure and the "50% threshold" technique to quantify event amplitudes and durations. Threshold was adjusted for each opening and all events were manually inspected before being included in analysis. Amplitude histograms used only events >1 ms to ensure that events had reached full amplitude. Missed short events due to the rise time of the filter were not accounted for. All amplitudes for a given voltage in a single patch were binned and fit with a Gaussian distribution, the mean of which represented the amplitude at that voltage.

Open-time distribution histograms were logarithmically binned, with the square root of the number of events (✓#evts) plotted against $\log_{10}$ duration. Histograms were fit with a sum of exponential probability density functions (PDF) of the form:

$$PDF = \sum_{i=1}^{N} \frac{a_i}{\tau_i} e^{\frac{-t}{\tau_i}}$$

Where N is the number of PDFs required to best fit the data, a_i is the proportional weighting of each PDF ($\sum a_i = 1$), τ_i is the time constant of each PDF and t is the time bin. Data were fit using the maximum likelihood method, with the minimum number of exponential PDFs required to best describe the data were used.

Statistical analysis:

All numerical values are expressed as mean ± S.D. Group sizes were not prespecified before acquisition of data. All inter-group statistical comparisons were decided before initial data had been obtained. Data were analysed with a Student's t-test or One-way ANOVA (GraphPad Software, San Diego, CA *).* All statistical comparisons that have been done are reported in the manuscript. A paired two -tailed t test was used to compare inhibition of current by added inhibitor,

while an unpaired two-tailed t test was used to compare the magnitude of inhibition of homomeric and heteromeric current by an inhibitor. An unpaired t-test was used to test cluster radius using GraphPad Prism 4.0 (GraphPad Software, San Diego, CA). Representative current traces were drawn using Origin 9.1 (Microcal Software Inc., Northampton, MA). Finally, reported statistical comparisons did not test a pre-specified null-hypothesis and are only descriptive.

Results

SK1 and IKCa subunits are derived from the same gene family of Ca^{2+}-dependent potassium channels, but functional homomeric channels display distinct pharmacological profiles that arise from sequence differences between channel isoforms. We have utilised possible changes in pharmacological response, together with point localization and FRET microscopy, to determine whether expression of human SK1 (hSK1) and human IKCa (hIKCa) in tsA-201 cells assemble as homomeric or heteromeric channels.

hSK1 and hIKCa co-clusters detected by STORM:

At the molecular level a functional heteromeric channel will be comprised of SK1 and IKCa channel alpha subunits in very close proximity. Structural studies of single voltage-gated and calcium-activated potassium channels predict that an assembled channel exhibits a diameter of ~10-15 nm (Doyle *et al.*, 1998; Jiang *et al.*, 2002; Wang and Sigworth, 2009). Imaging structures of this size using standard optical microscopy is restricted by diffraction, with a typical resolution of approximately ~250 nm. To probe structures below the resolution limit, complementary techniques, such as Stochastic Optical Reconstruction Microscopy (STORM) and Fluorescence Resonance Energy Transfer (FRET), can be applied to determine if hSK1 and hIKCa subunits associate with a proximity consistent with heteromeric channel formation when co-expressed in tsA-201 cells.

Cells transiently expressing untagged hSK1 and hIKCa subunits were fixed and processed for immunolabeling of each channel subunit. STORM imaging was conducted with total internal reflection fluorescence (TIRF) illumination at a depth of ~100-150 nm to capture fluorescent signals arising from proteins residing in the plasma membrane or immediate sub-plasma membrane compartment (Zhang *et al.*, 2016; Vivas *et al.*, 2017). STORM can be used to determine the location of proteins according to the detection of stochastic blinking of fluorophores upon return from a dark state to the ground state (Rust *et al.*, 2006; Bates *et al.*, 2007; van de Linde *et al.*, 2011). Each final STORM-TIRF image was derived from 20,000-35,000 individual images to capture a cloud of individual blinking events, followed by Gaussian filtering to define the spatial location of fluorophore-tagged channel proteins (Thunderstorm, ImageJ) (Ovesny *et al.*, 2014). The images were corrected for any drift or chromatic aberration by aligning 2-6 100 nm fiducial beads located within the field of view using affain registration (Lama) (Malkusch and Heilemann, 2016). The precision of localization was then measured using a least square-based localization algorithm (Thompson *et al.*, 2002). Through this process proteins could be localized with a precision of 37.1 ± 4.5 nm for hSK1 channels and 26.2 ± 4.2 nm for hIKCa channels (n=7).

STORM-TIRF images of tsA-201 cells co-expressing hSK1 and hIKCa channel subunits revealed a relatively uniform pattern of punctate immunolabeling for channels across the surface of the cell (Figure 1A). A morphological cluster analysis was applied to elucidate the spatial relationship between immunolabels (Lama) (Malkusch and Heilemann 2016). A minimum criterion corresponding to a 40 nm radius was used to define a cluster, given our estimated precision of SK1 and IKCa fluorescent signals of approximately 25-35 nm. This analysis indicated that cluster radii varied substantially (40-600 nm), but had a similar mean radius for hSK1 of 175 ± 113 (n=7) and for hIKCa of 170 ± 96 nm (n=7). Since the width of individual potassium channels is ~10-15 nm, the mean radius for hSK1 and hIKCa immunolabeled clusters is interpreted to reflect signals that arise from multiple channels (see Discussion).

Close examination of the distribution of immunolabels revealed that the vast majority of hSK1- and hIKCa-labeled clusters were in close apposition or partially overlapped with one another, with only a few isolated clusters (Figure 1B). After cluster centroids were identified, a nearest neighbor analysis indicated that the minimum distance between neighboring hSK1-hSKI clusters followed a normal distribution with a peak of 875 ± 68 nm (n=7) (Figure 1C). The nearest neighbor distance between hIKCa-hIKCa cluster centroids was also normally distributed with a peak of 975 ± 11 nm (n=7) (Figure 1D). However, a histogram plot of the hSK1-hIKCa nearest neighbors was skewed to the right with a peak of 205 ± 76 nm (n=7) (Figure 1E). These data would suggest no specific association between clusters of a given fluorophore-labeled subunit, but a preferred close association between hSK1-hIKCa clusters, as found in the overlap of fluorescent labels in Figure 1(A & B).

Fluorophore-tagged hSK1 and hIKCa channel subunits exhibit FRET

Spectral FRET imaging was used to examine if hSK1 and hIKCa subunits can physically associate with a proximity (<10 nm) expected for a heteromeric channel. Specifically, imaging for FRET was tested between a C-terminal eGFP-tagged SK1 subunit (donor) and a C-terminal mKate-tagged IKCa subunit (acceptor). Control recordings of fluorophore-tagged channels expressed in tsA-201 cells verified both tagged subunits generated the appropriate current when expressed alone and displayed block by apamin (hSK1) or TRAM-34 (hIKCa) (**Supplementary Figure 2**). When both constructs were co-expressed in tsA-201 cells, excitation with a 457 nm laser line yielded fluorescence emission consistent with FRET, as indicated by dual emission spectra for both hSK1-eGFP and hIKCa-mKate (Figure 2A). By comparison, excitation using a 561 nm laser line produced, as expected emission spectra of hIKCa-mKate alone (Figure 2B). Further, no FRET was detected in cells co-expressing eGFP-tagged hSK1 with mKate cDNA (Figure 2C & D), or in cells co-expressing mKate-tagged hIKCa with eGFP (Figure 2E & F). The ability to detect FRET between channel subunits expressed in homomeric assembly was tested by co-expressing hSK1 cDNAs tagged with eGFP or mKate (Figure 2G) or hIKCa cDNA tagged

with eGFP or mKate (Figure 2H). Together these data reveal high efficiency FRET between channel subunits co-expressed as either homomeric or heteromeric combinations in tsA-201 cells (Figure 2I). FRET measurements thus support the results obtained from STORM-TIRF analysis of a heteromeric assembly of hSK1 and hIKCa subunits.

Pharmacology of expressed currents

Previous work has shown that heteromeric assembly of alpha subunits from different channel isoforms can alter channel properties (Manganas and Trimmer, 2000; Akhtar *et al.*, 2002; Etxeberria *et al.*, 2004; Sokolov *et al.*, 2007; Al-Sabi *et al.*, 2010; Abi-Gerges *et al.*, 2011; Brueggemann *et al.*, 2011; Jenkins *et al.*, 2011). We used a pharmacological approach to compare the properties of homomeric hSK1 and hIKCa channels to those formed when subunits are co-expressed. Outside-out patches excised from tsA-201 cells expressing hSK1 channel subunits had inward-rectifying currents activated by 1 μM Ca^{2+} contained in the electrode solution, revealed by voltage ramps from -100 to +100 mV (Figure 3). As expected from previous studies, hSK1 current was inhibited by apamin (100 nM) (Figure 3A) or UCL1684 (100 nM) (Figure 3B), but was insensitive to TRAM-34 (10 μM) (Figure 3C) or charybdotoxin (Ctx) (100 nM) (Figure 3D). In contrast, excised outside-out patches from cells expressing hIKCa channel subunits displayed Ca^{2+}-dependent currents that exhibited various degrees of inward rectification. Extracellular application of TRAM-34 (10 μM) (Figure 4A) or Ctx (100 nM) (Figure 4B) blocked current, while the SK current inhibitors apamin (Figure 4C) and UCL1684 (Figure 4D) were without effect. These data demonstrate that homomeric hSK1 or hIKCa channel current display distinct pharmacology.

Co-expression of hSK1 and hIKCa channel subunits produced inward-rectifying current, revealed by a voltage ramp from -100 to 100 mV (Figure 5). Extracellular application of inhibitors to excised outside-out patches revealed a different pharmacology from that seen with homomeric channels. Application of apamin (100 nM) (Figure 5A) and UCL1684 (100 nM) (Figure 5B) had no significant effect on current, demonstrating that no homomeric hSK1 channels were formed. In contrast,

current was only partially inhibited by TRAM-34 (10 μM) (Figure 5C) or Ctx (100 nM) (Figure 5D). For example, addition of TRAM-34 (10 μM) inhibited 92 ± 1.4% of homomeric hIKCa current at -60 mV (n=7, P=0.0001), where only 54.6 ± 9.1% inhibition was observed of heteromeric hSK1-hIKCa current (n=10, P=0.0001) (P value of difference in block). A similar change in sensitivity to Ctx was noted, where homomeric hIKCa current was blocked by 95.5 ± 11% by 100 nM Ctx (n=4, P=0.0001) but only a 30.6 ± 23.1%% block was observed of heteromeric hSK1-hIKCa current (n=7, P=0.0001).

Inhibition by TRAM-34 was further investigated by generation of concentration-inhibition relationships from outside-out patches excised from cells expressing only hIKCa channel subunits and from those co-expressing hSK1 and hIKCa channel subunits. TRAM-34-mediated inhibition of homomeric hIKCa current was best fit by a single Hill coefficient, with an IC_{50} of 41 nM, with a maximum inhibition of 92% (Figure 6A & C). In contrast, the concentration-inhibition relationship for current from cells co-expressing hSK1 and hIKCa channel subunits showed that sensitivity of heteromeric channels is reduced, with an IC_{50} of 557 nM (Figure 6B & C). In addition, only approximately 55% of the current was sensitive to TRAM-34 (Figure 6C). These data confirm that functional heteromeric channels displayed a unique pharmacology.

Single-channel properties of expressed channels

The single-channel properties of expressed homomeric SK or IKCa channels have been reported under various ionic conditions. SK channels display a single-channel conductance of approximately 10-20 pS under isotonic K^+ conditions (Kohler *et al.*, 1996; Hirschberg *et al.*, 1999; Goodchild *et al.*, 2009). In contrast, IKCa channels display a single-channel conductance of approximately 11-50 pS (Ishii *et al.*, 1997; Joiner *et al.*, 1997; Logsdon *et al.*, 1997; Vogalis *et al.*, 2002; Neylon *et al.*, 2004; Wulff *et al.*, 2007; King *et al.*, 2015). However, differences in experimental conditions makes comparison difficult. Expressed homomeric hSK1 channels exhibited a conductance of 20 pS under isotonic 150 mM K^+ conditions (10 out 28 patches

contained channel activity) (Figure 7A & B). In contrast, homomeric hIKCa channels displayed a conductance of 53 pS under identical conditions (7 out 15 patches contained channel activity) (Figure 7A & B). The single-channel conductance of heteromeric channels was different from that observed for homomeric channels. Heteromeric hSK1-hIKCa channels displayed a conductance of 36 pS, intermediate between the values of each homomeric channel (7 out 15 patches contained channel activity) (Figure 7A & B). The open state kinetics of hSK and hIKCa channels exhibited marked differences. hSK1 channels exhibited a biexponential distribution with open time constants of 3 and 23 ms (Figure 7C). In contrast, hIKCa openings were clearly more brief, exhibiting a single exponential distribution with open time constant of 3 ms (Figure 7C). The open state kinetics of heteromeric channels was closer to those seen with homomeric hIKCa channels rather than hSK1 channels. Openings were best described by a single exponential distribution of time constant of 5 ms (Figure 7C).

Discussion

Formation of heteromeric channels adds more diversity to an already extensive population of functional K^+ channels. It has been demonstrated that SK channel subunits preferentially form heteromeric channels, with no evidence of a mixture of heteromeric and homomeric channels when expressed in a heterologous system (Church *et al.*, 2015). Such heterogeneity is seen with the SK3 variant SK3-1C, which can co-assemble with all SK channel subunits and IKCa subunits to prevent expression in heterologous cells (Kolski-Andreaco et al. 2004). Obviously, this property of forming heteromeric channels can only be fulfilled *in situ* if subunits are expressed and reside in the same subcellular compartment. It is now documented that IKCa channels are expressed in both peripheral and central neurons, and are present in cells that express both SK and IKCa channel subunits (Neylon *et al.*, 2004; Mongan *et al.*, 2005; Nguyen *et al.*, 2007; Engbers *et al.*, 2012; King *et al.*, 2015; Turner *et al.*, 2015; Tiwari *et al.*, 2018).

The association between different proteins and the potential formation of heteromeric channels has been studied before through STORM in the case of KCNQ and Cav1.2/TRPV channels (Zhang *et al.*, 2016), Cav1.3 and BK potassium channels (Vivas *et al.*, 2017), and calcium channels in relation to presynaptic release machinery (Dani *et al.*, 2010).

Analysis of the STORM data yielded cluster radii ranging between 40-600 nm of hSK1 and hIKCa channel subunits. It is important to recognize that in these STORM experiments, we are not reporting on the localization of the channels themselves but rather the signal emitted from fluorophore-conjugated secondary antibodies. The number of primary or secondary antibodies associated with a single channel are unknown but could reflect at least 4 antibody complexes given the potential to label any of 4 subunits in a homomeric channel. Similarly, the spatial orientation of antibodies and fluorophores is unknown. Given that both primary and secondary antibodies are ~5-10 nm in size and fluorophores 2-3 nm (i.e. Alexa 657), it is conceivable that an antibody complex oriented lateral to the imaging plane could add another ~25 nm signal to the side of a single potassium channel. Thus, with a lateral dimension of 10-15 nm for a channel together with ~50 nm for an assumed total width of fluorophore signals, the potential minimum cluster size increases to 65 nm. The smallest clusters of 40 nm detected here might then imply signals arising from single channels. Nevertheless, we recognize that this is the extreme case, suggesting that cluster dimensions more likely reflect signals associated with multiple ion channel-fluorophore localizations.

STORM imaging revealed a close association between hSK1 and hIKCa-related clusters (Figure 1A & B). Analysis of the Euclidean distance between nearest neighbors indicates that hSK1 and hIKCa subunits were preferentially associated (Figure 1E). Further, a mean value of 205 nm distance between the centroids of hSK1-hIKCa clusters (Figure 1E) is close to the mean value of ~170 nm for hSK1 and hIKCa cluster radii (Figure 1C). These measures could account for the extensive overlap detected in adjacent hSK1 and hIKCa fluorescent clusters (Figure 1B), results

consistent with a very close association between hSK1-hIKCa subunits and heteromeric channel formation. We obtained further support for this conclusion by using FRET that depends on an interaction between a pair of fluorophores positioned within 10 nm distance (Bajar et al. 2016). Thus, the ability for hSK1-eGFP to enable FRET with hIKCa-mKate is again consistent with an extremely close association between hSK1 and hIKCa channel subunits expected for heteromeric channel formation.

The presence of functional heteromeric channels was demonstrated using pharmacological inhibition of expressed channel current. The presented data showed that co-expression of hSK1 and hIKCa channel subunits produced current that exhibited a pharmacological profile different from that observed with expressed homomeric channel current. A prominent difference between heteromeric hSK1-hIKCa channel current and homomeric hIKCa channel current is the sensitivity to inhibition by TRAM-34. Concentration-inhibition relationships showed that heteromeric current is more than 10-fold less sensitive to the organic inhibitor and that the maximum inhibition is significantly reduced (Figure 6C). Importantly, application of apamin to current remaining in TRAM-34 was without effect (data not shown). These data suggest that there was not a detectable population of homomeric hSK1 channels that could be identified by pharmacology, and that hSK1 subunits prefer to combine with hIKCa subunits to form heteromeric channels. Similarly, the reduced maximum inhibition observed with TRAM-34 inhibition of heteromeric channels indicates that there was not a detectable population of homomeric hIKCa channels, and again suggests that this subunit prefers to form functional heteromeric channels.

It is clear that formation of heteromeric channels between SK1 and IKCa subunits changes sensitivity to one of the most specific blockers of IKCa channel current. TRAM-34 is a triarylmethane drug developed through modification of clotrimazole that typically exhibits an IC_{50} in the range of 25 nM (Figure 6C) (Wulff *et al.*, 2000, 2007; Jenkins *et al.*, 2013). Pharmacological tests suggest a working concentration of up 1 µM TRAM-34 can be applied in most tissues without

significant secondary block of other channels (Jenkins *et al.*, 2013). While IKCa channel expression has been widely reported in cells of the immune system and peripheral enteric neurons (Neylon *et al.*, 2004; Wulff *et al.*, 2007), the expression and role for these channels in central neurons has only recently come to light (Engbers *et al.*, 2012; Turner *et al.*, 2015, 2016). The apparent sensitivity to TRAM-34 can also differ between neuronal cell types, with the parallel fiber-evoked afterhyperpolarization (AHP) in cerebellar Purkinje cells blocked by 100 nM TRAM-34 (Engbers *et al.*, 2012), while reduction of the slow AHP in hippocampal pyramidal cells required 5 µM TRAM-34 (King *et al.*, 2015; Sahu *et al.*, 2017; Tiwari *et al.*, 2018). It is possible that these differences reflect channel subunit expression or stoichiometry.

Inhibition of SK channel current by apamin displays positive cooperativity, but only when two subunits that can bind apamin are adjacent to each other in the channel tetramer (Lamy *et al.*, 2010). Apamin is a negative allosteric modulator of SK channels that binds to both the outer turret of the channel and the extracellular loop between transmembrane domains S3 and S4 (Nolting *et al.*, 2007; Lamy *et al.*, 2010; Weatherall *et al.*, 2011) and modulates channel gating through an asparagine residue that is distant from the conducting pore (Lamy *et al.*, 2010). Importantly, the high affinity binding site for apamin requires that two subunits that can bind the toxin are adjacent in the tetramer because the S3-S4 extracellular loop is donated to the adjacent subunit to allow apamin to bind to both the outer pore turret and extracellular loop (Weatherall *et al.*, 2011). Co-expression of hSK1 and hIKCa channel subunits produces a heteromeric channel that proved to be insensitive to apamin. These data indicate that the heteromeric channel always forms with either only one hSK1 subunit and three hIKCa subunits, or two hSK1 subunits that are not adjacent to each other in the tetramer and alternate with IKCa around the tetramer.

Inhibition of homomeric IKCa channel current by TRAM-34 is disrupted when threonine 250 in the pore loop is mutated to serine, and/or valine 275 in transmembrane domain S6 is mutated to alanine, residues that are in equivalent positions in SK3 and SK1 (Wulff *et al.*, 2001). Interaction

with T250 might suggest that TRAM-34 is an open channel blocker, although that has yet to be determined. It has been suggested that the pyrazole ring of TRAM-34 uses the side chains of V275 on each subunit to be orientated for interaction with T250 of one subunit (Brown *et al.*, 2018). This proposal suggests that high sensitivity to block of IKCa channel current by TRAM-34 requires all 4 IKCa channel subunits. Therefore, it is to be expected that a heteromeric SK1-IKCa channel current will be less sensitive to inhibition by TRAM-34. Finally, the observed reduced maximum inhibition of heteromeric SK1-IKCa channel current by TRAM-34 (Figure 6C) would be expected with a predicted reduction in binding affinity resulting from the presence of SK1 subunits within the heteromeric tetramer.

The STORM and FRET data and pharmacological profile of co-expressed channel subunits thus suggest that SK1 and IKCa channel subunits prefer to form functional heteromeric channels of fixed stoichiometry and arrangement of subunits within the tetramer. This provides a heteromeric Ca^{2+}-activated K^+ channel that displays unique single-channel and pharmacological properties.

Acknowledgements

We gratefully acknowledge J. Forden for technical assistance in cell culture preparations.

Author Contributions

G.S. prepared fluorophore-tagged constructs and conducted FRET, G.S., R-M.W., and P.C. performed STORM imaging and analysis and J.H., G.S., B.S.J.H., L.G., G.V. did electrophysiology. N.V.M, G.S. and R.W.T. wrote the manuscript. N.V.M., D.N.S., R.W.T. and P.C. supervised the studies and provided necessary reagents and supplies.

References

Abi-Gerges N, Holkham H, Jones EMC, Pollard CE, Valentin J-P, and Robertson GA (2011) hERG subunit composition determines differential drug sensitivity. *Br J Pharmacol* **164**:419–432.

Akhtar S, Shamotienko O, Papakosta M, Ali F, and Dolly JO (2002) Characteristics of Brain Kv1 Channels Tailored to Mimic Native Counterparts by Tandem Linkage of α Subunits: implications for K^+ channelopathies. *J Biol Chem* **277**:16376–16382.

Al-Sabi A, Shamotienko O, Dhochartaigh SN, Muniyappa N, Le Berre M, Shaban H, Wang J, Sack JT, and Oliver Dolly J (2010) Arrangement of Kv1 α subunits dictates sensitivity to tetraethylammonium. *J Gen Physiol* **136**:273–282, Rockefeller University Press.

Asmara H, Micu I, Rizwan AP, Sahu G, Simms BA, Zhang FX, Engbers JDT, Stys PK, Zamponi GW, and Turner RW (2017) A T-type channel-calmodulin complex triggers αCaMKII activation. *Mol Brain* **10**:37.

Bajar BT, Lam AJ, Badiee RK, Oh YH, Chu J, Zhou XX, Kim N, Kim BB, Chung M, Yablonovitch AL, Cruz BF, Kulalert K, Tao JJ, Meyer T, Su XD, and Lin MZ (2016) Fluorescent indicators for simultaneous reporting of all four cell cycle phases. *Nat Methods* **13**:993-996.

Balut CM, Hamilton KL, and Devor DC (2012) Trafficking of intermediate ($K_{Ca}3.1$) and small ($K_{Ca}2.x$) conductance, Ca^{2+}-activated K^+ channels: a novel target for medicinal chemistry efforts? *ChemMedChem* **7**:1741–1755.

Bates M, Huang B, Dempsey GT, and Zhuang X (2007) Multicolor super-resolution imaging with photo-switchable fluorescent probes. *Science* **317**:1749–1753.

Bond CT, Herson PS, Strassmaier T, Hammond R, Stackman R, Maylie J, and Adelman JP (2004) Small conductance Ca^{2+}-activated K^+ channel knock-out mice reveal the identity of calcium-dependent afterhyperpolarization currents. *J Neurosci* **24**:5301–5306.

Bowden SE, Fletcher S, Loane DJ, and Marrion NV (2001) Somatic colocalization of rat SK1 and D class ($Ca_V1.3$) L-type calcium channels in rat CA1 hippocampal pyramidal neurons. *J Neurosci* **21**:RC175.

Brown BM, Pressley B, and Wulff H (2018) KCa3.1 Channel Modulators as Potential Therapeutic Compounds for Glioblastoma. *Curr Neuropharmacol* **16**:618–626.

Brueggemann LI, Mackie AR, Martin JL, Cribbs LL, and Byron KL (2011) Diclofenac distinguishes among homomeric and heteromeric potassium channels composed of KCNQ4 and KCNQ5 subunits. *Mol Pharmacol* **79**:10–23.

Church TW, Weatherall KL, Correa SA, Prole DL, Brown JT, and Marrion NV (2015) Preferential assembly of heteromeric small conductance calcium-activated potassium channels. *Eur J Neurosci* **41**:305–315.

Dani A, Huang B, Bergan J, Dulac C, and Zhuang XW (2010) Super-resolution imaging of chemical synapses in the brain. *Neuron* **68**:843–856.

Doyle DA, Cabral JM, Pfuetzner RA, Kuo AL, Gulbis JM, Cohen SL, Chait BT, and MacKinnon R (1998) The structure of the potassium channel: Molecular basis of K^+ conduction and selectivity. *Science* **280**:69–77.

Engbers JD, Anderson D, Asmara H, Rehak R, Mehaffey WH, Hameed S, McKay BE, Kruskic M, Zamponi GW, and Turner RW (2012) Intermediate conductance calcium-activated potassium channels modulate summation of parallel fiber input in cerebellar Purkinje cells. *Proc Natl Acad Sci U S A* **109**:2601–2606.

Erkens GB, Hanelt I, Goudsmits JMH, Slotboom DJ and Oijen AMV (2013) Unsynchronized subunit motion in single trimeric sodium-coupled aspartate transporters. *Nature* 502:119-123. Etxeberria A, Santana-Castro I, Regalado MP, Aivar P, and Villarroel A (2004) Three mechanisms underlie KCNQ2/3 heteromeric potassium M-channel potentiation. *J Neurosci* **24**:9146–9152.

Goodchild SJ, Lamy C, Seutin V, and Marrion NV (2009) Inhibition of $K_{Ca}2.2$ and $K_{Ca}2.3$ channel currents by protonation of outer pore histidine residues. *J Gen Physiol* **134**:295–308.

Hancock JM, Weatherall KL, Choisy SC, James AF, Hancox JC, and Marrion NV (2015) Selective activation of heteromeric SK channels contributes to action potential repolarization in mouse atrial myocytes. *Heart Rhythm* **12**:1003–1015.

Hirschberg B, Maylie J, Adelman JP, and Marrion NV (1999) Gating properties of single SK channels in hippocampal CA1 pyramidal neurons. *Biophys J* **77**:1905–1913.

Ishii TM, Silvia C, Hirschberg B, Bond CT, Adelman JP, and Maylie J (1997) A human intermediate conductance calcium-activated potassium channel. *Proc Natl Acad Sci U S A* **94**:11651–11656.

Jenkins DP, Yu W, Brown BM, Lojkner LD, and Wulff H (2013) Development of a QPatch Automated Electrophysiology Assay for Identifying $K_{Ca}3.1$ Inhibitors and Activators. *Assay Drug Dev Technol* **11**:551–560.

Jenkins PM, McIntyre JC, Zhang L, Anantharam A, Vesely ED, Arendt KL, Carruthers CJL, Kerppola TK, Iñiguez-LluhÍ JA, Holz RW, Sutton MA, and Martens JR (2011) Subunit-Dependent Axonal Trafficking of Distinct α Heteromeric Potassium Channel Complexes. *J Neurosci* **31**:13224–13235.

Jiang YX, Lee A, Chen JY, Cadene M, Chait BT, and MacKinnon R (2002) Crystal structure and mechanism of a calcium-gated potassium channel. *Nature* **417**:515–522.

Joiner WJ, Wang LY, Tang MD, and Kaczmarek LK (1997) hSK4, a member of a novel subfamily of calcium-activated potassium channels. *Proc Natl Acad Sci U S A* **94**:11013–11018.

King B, Rizwan AP, Asmara H, Heath NC, Engbers JD, Dykstra S, Bartoletti TM, Hameed S, Zamponi GW, and Turner RW (2015) IKCa channels are a critical determinant of the slow AHP in CA1 pyramidal neurons. *Cell Rep* **11**:175–182.

Kohler M, Hirschberg B, Bond CT, Kinzie JM, Marrion NV, Maylie J, and Adelman JP (1996) Small-conductance, calcium-activated potassium channels from mammalian brain. *Science* **273**:1709–1714.

Kolski-Andreaco A, Tomita H, Shakkottai VG, Gutman GA, Cahalan MD, Gargus JJ, and Chandy KG. (2004) SK3-1C, a dominant-negative suppressor of SKCa and IKCa channels. J Biol Chem. 2004 Feb 20;279(8):6893-904.

Lamy C, Goodchild SJ, Weatherall KL, Jane DE, Liegeois JF, Seutin V, and Marrion NV (2010) Allosteric block of $K_{Ca}2$ channels by apamin. *J Biol Chem* **285**:27067–27077.

Logsdon NJ, Kang J, Togo JA, Christian EP, and Aiyar J (1997) A novel gene, hK_{Ca}4, encodes the calcium-activated potassium channel in human T lymphocytes. *J Biol Chem* **272**:32723–32726.

Malkusch S, and Heilemann M (2016) Extracting quantitative information from single-molecule super-resolution imaging data with LAMA - LocAlization Microscopy Analyzer. *Sci Rep* **6**:34486.

Manganas LN, and Trimmer JS (2000) Subunit composition determines K_V1 potassium channel surface expression. *J Biol Chem* **275**:29685–29693.

Mongan LC, Hill MJ, Chen MX, Tate SN, Collins SD, Buckby L, and Grubb BD (2005) The distribution of small and intermediate conductance calcium-activated potassium channels in the rat sensory nervous system. *Neuroscience* **131**:161–175.

Neylon CB, Nurgali K, Hunne B, Robbins HL, Moore S, Chen MX, and Furness JB (2004) Intermediate-conductance calcium-activated potassium channels in enteric neurones of the mouse: pharmacological, molecular and immunochemical evidence for their role in mediating the slow afterhyperpolarization. *J Neurochem* **90**:1414–1422.

Nguyen TV, Matsuyama H, Baell J, Hunne B, Fowler CJ, Smith JE, Nurgali K, and Furness JB (2007) Effects of compounds that influence IK (KCNN4) channels on afterhyperpolarizing potentials, and determination of IK channel sequence, in guinea pig enteric neurons. *J Neurophysiol* **97**:2024–2031.

Nolting A, Ferraro T, D'Hoedt D, and Stocker M (2007) An amino acid outside the pore region influences apamin sensitivity in small conductance Ca^{2+}-activated K^+ channels. *J Biol Chem* **282**:3478–3486.

Ovesny M, Krizek P, Borkovec J, Svindrych Z, and Hagen GM (2014) ThunderSTORM: a comprehensive ImageJ plug-in for PALM and STORM data analysis and super-resolution imaging. *Bioinformatics* **30**:2389–2390.

Rust MJ, Bates M, and Zhuang X (2006) Sub-diffraction-limit imaging by stochastic optical reconstruction microscopy (STORM). *Nat Methods* **3**:793–795.

Sahu G, Asmara H, Zhang FX, Zamponi GW, and Turner RW (2017) Activity-dependent facilitation of Ca_V1.3 calcium channels promotes K_{Ca}3.1 activation in hippocampal neurons. *J Neurosci* **37**:11255–11270.

Schindelin J, Arganda-Carreras I, Frise E, Kaynig V, Longair M, Pietzsch T, Preibisch S, Rueden C, Saalfeld S, Schmid B, Tinevez JY, White DJ, Hartenstein V, Eliceiri K, Tomancak P, and Cardona A (2012) Fiji: an open-source platform for biological-image analysis. *Nat Methods* **9**:676–682.

Sokolov MV, Shamotienko O, Dhochartaigh SN, Sack JT, and Dolly JO (2007) Concatemers of brain K_V1 channel alpha subunits that give similar K^+ currents yield pharmacologically distinguishable heteromers. *Neuropharmacology* **53**:272–282.

Stocker M, Krause M, and Pedarzani P (1999) An apamin-sensitive Ca^{2+}-activated K^+ current in hippocampal pyramidal neurons. *Proc Natl Acad Sci U S A* **96**:4662–4667.

Thompson RE, Larson DR, and Webb WW (2002) Precise nanometer localization analysis for individual fluorescent probes. *Biophys J* **82**:2775–2783.

Tiwari MN, Mohan S, Biala Y, and Yaari Y (2018) Differential contributions of Ca^{2+} -activated K^+

channels and Na^+ /K^+ -ATPases to the generation of the slow afterhyperpolarization in CA1 pyramidal cells. *Hippocampus* **28**:338–357.

Turner RW, Asmara H, Engbers JD, Miclat J, Rizwan AP, Sahu G, and Zamponi GW (2016) Assessing the role of IKCa channels in generating the sAHP of CA1 hippocampal pyramidal cells. *Channels* **10**:313-319.

Turner RW, Kruskic M, Teves M, Scheidl-Yee T, Hameed S, and Zamponi GW (2015) Neuronal expression of the intermediate conductance calcium-activated potassium channel $K_{Ca}3.1$ in the mammalian central nervous system. *Pflugers Arch* **467**:311–328.

van de Linde S, Loschberger A, Klein T, Heidbreder M, Wolter S, Heilemann M, and Sauer M (2011) Direct stochastic optical reconstruction microscopy with standard fluorescent probes. *Nat Protoc* **6**:991–1009.

Vivas O, Moreno CM, Santana LF, and Hille B (2017) Proximal clustering between BK and $Ca_V1.3$ channels promotes functional coupling and BK channel activation at low voltage. *Elife* **6**.

Vogalis F, Harvey JR, Neylon CB, and Furness JB (2002) Regulation of K^+ channels underlying the slow afterhyperpolarization in enteric afterhyperpolarization-generating myenteric neurons: role of calcium and phosphorylation. *Clin Exp Pharmacol Physiol* **29**:935–943.

Wang L, and Sigworth FJ (2009) Structure of the BK potassium channel in a lipid membrane from electron cryomicroscopy. *Nature* **461**:292–295.

Weatherall KL, Goodchild SJ, Jane DE, and Marrion NV (2010) Small conductance calcium-activated potassium channels: from structure to function. *Prog Neurobiol* **91**:242–255.

Weatherall KL, Seutin V, Liegeois JF, and Marrion NV (2011) Crucial role of a shared extracellular loop in apamin sensitivity and maintenance of pore shape of small-conductance calcium-activated potassium (SK) channels. *Proc Natl Acad Sci U S A* **108**:18494–18499.

Wulff H, Gutman GA, Cahalan MD, and Chandy KG (2001) Delineation of the clotrimazole/TRAM-34 binding site on the intermediate conductance calcium-activated potassium channel, IKCa1. *J Biol Chem* **276**:32040–32045.

Wulff H, Kolski-Andreaco A, Sankaranarayanan A, Sabatier JM, and Shakkottai V (2007) Modulators of small- and intermediate-conductance calcium-activated potassium channels and their therapeutic indications. *Curr Med Chem* **14**:1437–1457.

Wulff H, Miller MJ, Hansel W, Grissmer S, Cahalan MD, and Chandy KG (2000) Design of a potent and selective inhibitor of the intermediate-conductance Ca^{2+}-activated K^+ channel, IKCa1: a potential immunosuppressant. *Proc Natl Acad Sci U S A* **97**:8151–8156.

Zhang J, Carver CM, Choveau FS, and Shapiro MS (2016) Clustering and Functional Coupling of Diverse Ion Channels and Signaling Proteins Revealed by Super-resolution STORM Microscopy in Neurons. *Neuron* **92**:461–478.

Financial support: This work was supported by the British Heart Foundation (N.V.M) and a Canadian Institutes for Health Research Operating Grant (R.W.T.). Postdoctoral support (G.S.) was provided by an Eyes High Fellowship (University of Calgary) and Alberta Innovates - Health Solutions (AI-HS) Fellowship. B.S.J.H was part supported by the Cystic Fibrosis Trust. R.W.T. is an AI-HS Scientist.

Figure 1. STORM imaging reveals close apposition and overlap between clusters of fluorescent tagged hSK1 and hIKCa channels expressed in tsA-201 cells.

A, B. Low magnification immunofluorescence images of hSK1 (red) and hIKCa (green) channels co-expressed in tsA-201 cells (**A**), with indicated regions-of-interest (ROIs) expanded below (**B**). Clusters of fluorescent tags localized by STORM imaging and analysis are often overlapping (open blue arrows), closely opposed (solid blue arrow) or in some cases as overlapping signals for hIKCa (solid white arrow) or hSK1 (open white arrow). Scale bars, **A,** 5 μm, **B,** 500 nm. **C-E.** Gaussian distributed histogram plots of the minimum nearest-neighbour Euclidean distances between centroids of neighboring clusters for the indicated pairs of labels (bin width, 25 nm).

Figure 2. hSK1 channels associate with hIKCa channels to support FRET.

Fluorescence spectral confocal images of tsA-201 cells expressing combinations of constructs for hSK1-eGFP (donor molecule) and hIKCa-mKate (acceptor molecule) excited at either 457 nm or 561 nm. The associated plots show the average emission spectrum for each condition obtained from 30-40 cells from 3-4 independent experiments. Vertical lines denote the laser line of excitation. **A, B.** Excitation at 457 nm for cells co-expressing hSK1-eGFP and hIKCa-mKate channels induced FRET, as indicated by a dual emission spectra for eGFP (**A**) due to a direct excitation of eGFP and for mKate through energy transfer, as compared to only an hIKCa-mKate emission spectra when excited at 561 nm (**B**). **C-F**. No FRET is detected in cell co-expressing hSK1-eGFP channels and mKate cDNA (**C, D**), or in cells co-expressing hIKCa-mKate channels

and eGFP cDNA (**E, F**). **G, H.** FRET measurements evoked at 457 nm in tsA-201 cells expressing hSK1-eGFP and hSK1-mKate (**G**) or cells expressing hIKCa-eGFP and hIKCa-mKate (**H**). I. Mean bar plots of FRET efficiency between the indicated pairs of expressed cDNAs when excited at 457 nm. High efficiency FRET emissions are detected for homomeric and heteromeric co-expressions. Scale bars refer to all panels, 20 µm.

Figure 3. Pharmacology of homomeric hSK1 channel current. Membrane currents evoked by a voltage ramp from -100 mV to +100 mV (1 second duration) from outside-out patches excised from cells transiently expressing hSK1 subunits. hSK1-mediated current was inhibited by both apamin (100 nM) (n=9) (**A**) and UCL1684 (100 nM) (n=13) (**B**), but not affected by TRAM-34 (10 µM) (n=7) (**C**) or Ctx (100 nM) (n=5) (**D**). Inset in **C** shows subsequent addition of UCL1684 (100 nM) inhibited current not affected by TRAM-34, while inset in **D** illustrates subsequent block of Ctx-insensitive hSK1 current by apamin.

Figure 4. Pharmacology of homomeric hIKCa channel current. Membrane currents evoked by a voltage ramp from -100 mV to +100 mV (1 second duration) from outside-out patches excised from cells transiently expressing hIKCa subunits. hSK1-mediated current was completely inhibited by both TRAM-34 (10 µM) (n=7) (**A**) and Ctx (100 nM) (n=4) (**B**), but not affected by apamin (100 nM) (n=9) (**C**) or UCL1684 (100 nM) (n=6) (**D**). Insets in **C** and **D** show that subsequent addition of TRAM-34 (10 µM) inhibits IKCa current that is insensitive to the SK current inhibitors apamin (**C**) and UCL1684 (**D**).

Figure 5. Pharmacology of heteromeric hSK1-hIKCa channel current. Membrane currents evoked by a voltage ramp from -100 mV to +100 mV (1 second duration) from outside-out patches excised from cells transiently expressing both hSK1 and hIKCa subunits. hSK1-IKCa-mediated current was partially inhibited by both TRAM-34 (10 µM) (n=10) (**A**) and Ctx (100 nM) (n=7) (**B**), but not affected by apamin (100 nM) (n=7) (**C**) or UCL1684 (n=12) (100 nM) (**D**). Insets in **C** and

D show that subsequent addition of TRAM-34 (10 μM) inhibits hSK1-hIKCa current that is insensitive to the SK current inhibitors apamin (**C**) and UCL1684 (**D**).

Figure 6. Comparison of the sensitivity to inhibition by TRAM-34 of homomeric IKCa current and heteromeric hSK1-hIKCa current. **A.** Membrane currents evoked by a voltage ramp from -100 mV to +100 mV (1 second duration) from an outside-out patch excised from a cell transiently expressing only hIKCa subunits. Current was inhibited in a concentration-dependent manner by increasing concentrations of TRAM-34. **B.** Ramp currents evoked from an outside-out patch excised from a cell co-expressing hSK1 and hIKCa subunits. Evoked current was progressively inhibited by increasing concentrations of TRAM-34. **C.** Concentration-inhibition relationships for TRAM-34-mediated inhibition of homomeric IKCa channel current (●) (n=7) and heteromeric hSK1-hIKCa channel current (○) (n=10). Homomeric current was inhibited by TRAM-34 with an IC_{50} of 41 nM, while heteromeric current was less sensitive, being inhibited by TRAM-34 with an IC_{50} of 557 nM. In addition, the maximum inhibition of heteromeric current was reduced when compared with inhibition of homomeric current.

Figure 7. Single-channel properties of homomeric and heteromeric channels. **A.** Membrane current traces from inside-out patches excised from cells expressing hSK1 (left), hSK1-hIKCa (center) and hIKCa (right) subunits. **B.** Single-channel amplitudes were plotted against voltage to obtain conductance estimates for each channel complement, with hSK1 channels exhibiting a conductance of 20 pS (n=3), hIKCa channels displaying a conductance of 53 pS (n=3) and heteromeric hSK1-hIKCa channels exhibiting an intermediate conductance of 36 pS (n=4). **C.** Summed open state kinetics differed between channel subtypes, with hSK1 displaying a bi-exponential open time distribution of time constants (τ) 3.4 and 22.5 ms. Homomeric hIKCa channels exhibited a mono-exponential open time distribution of time constant (τ) 2.7 ms. Open state kinetics of heteromeric hSK1-hIKCa channels were best described by a single exponential distribution of time constant (τ) 4.9 ms.

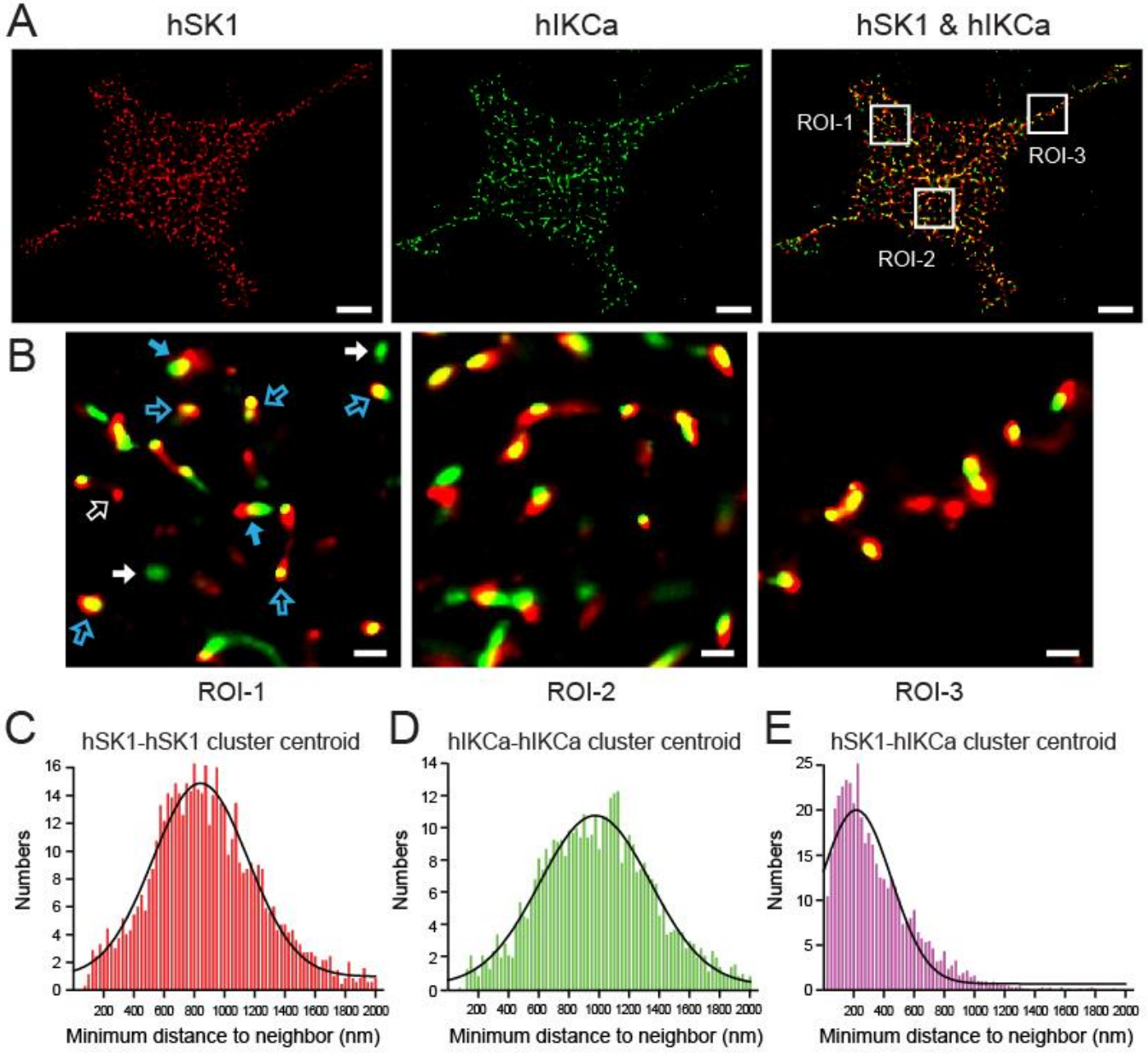
A
hSK1
hIKCa
hSK1 & hIKCa
ROI-1
ROI-2
ROI-3
B
ROI-1
ROI-2
ROI-3
C
hSK1-hSK1 cluster centroid
Numbers
Minimum distance to neighbor (nm)
D
hIKCa-hIKCa cluster centroid
Numbers
Minimum distance to neighbor (nm)
E
hSK1-hIKCa cluster centroid
Numbers
Minimum distance to neighbor (nm)

Figure 1

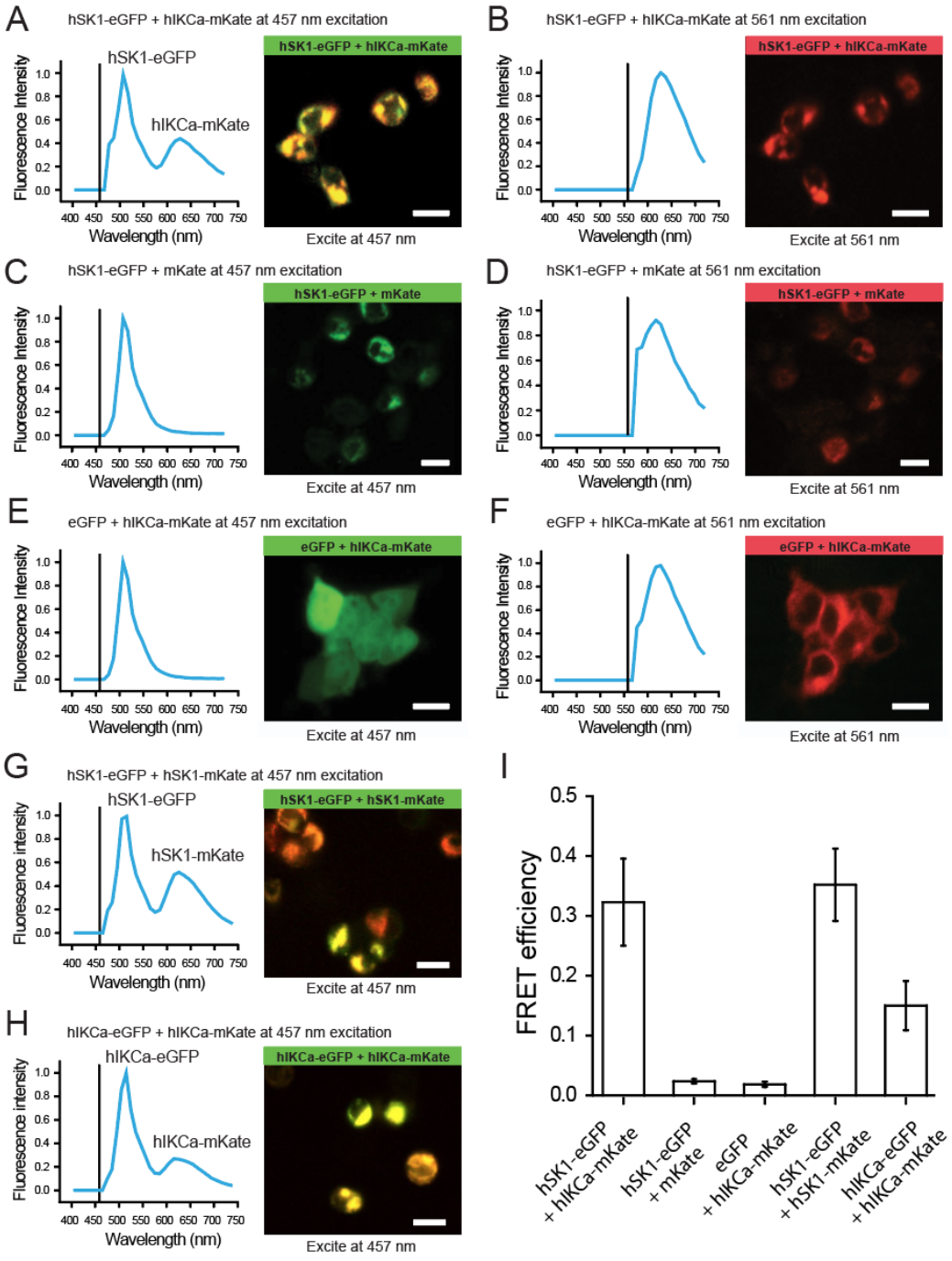
A
hSK1-eGFP + hIKCa-mKate at 457 nm excitation
hSK1-eGFP
hIKCa-mKate
Fluorescence Intensity
Wavelength (nm)
hSK1-eGFP + hIKCa-mKate
Excite at 457 nm
B
hSK1-eGFP + hIKCa-mKate at 561 nm excitation
Excite at 561 nm
C
hSK1-eGFP + mKate at 457 nm excitation
hSK1-eGFP + mKate
D
hSK1-eGFP + mKate at 561 nm excitation
E
eGFP + hIKCa-mKate at 457 nm excitation
eGFP + hIKCa-mKate
F
eGFP + hIKCa-mKate at 561 nm excitation
G
hSK1-eGFP + hSK1-mKate at 457 nm excitation
hSK1-mKate
hSK1-eGFP + hSK1-mKate
H
hIKCa-eGFP + hIKCa-mKate at 457 nm excitation
hIKCa-eGFP
hIKCa-mKate
I
FRET efficiency
hSK1-eGFP + hIKCa-mKate
hSK1-eGFP + mKate
eGFP + hIKCa-mKate
hSK1-eGFP + hSK1-mKate
hIKCa-eGFP + hIKCa-mKate

Figure 2

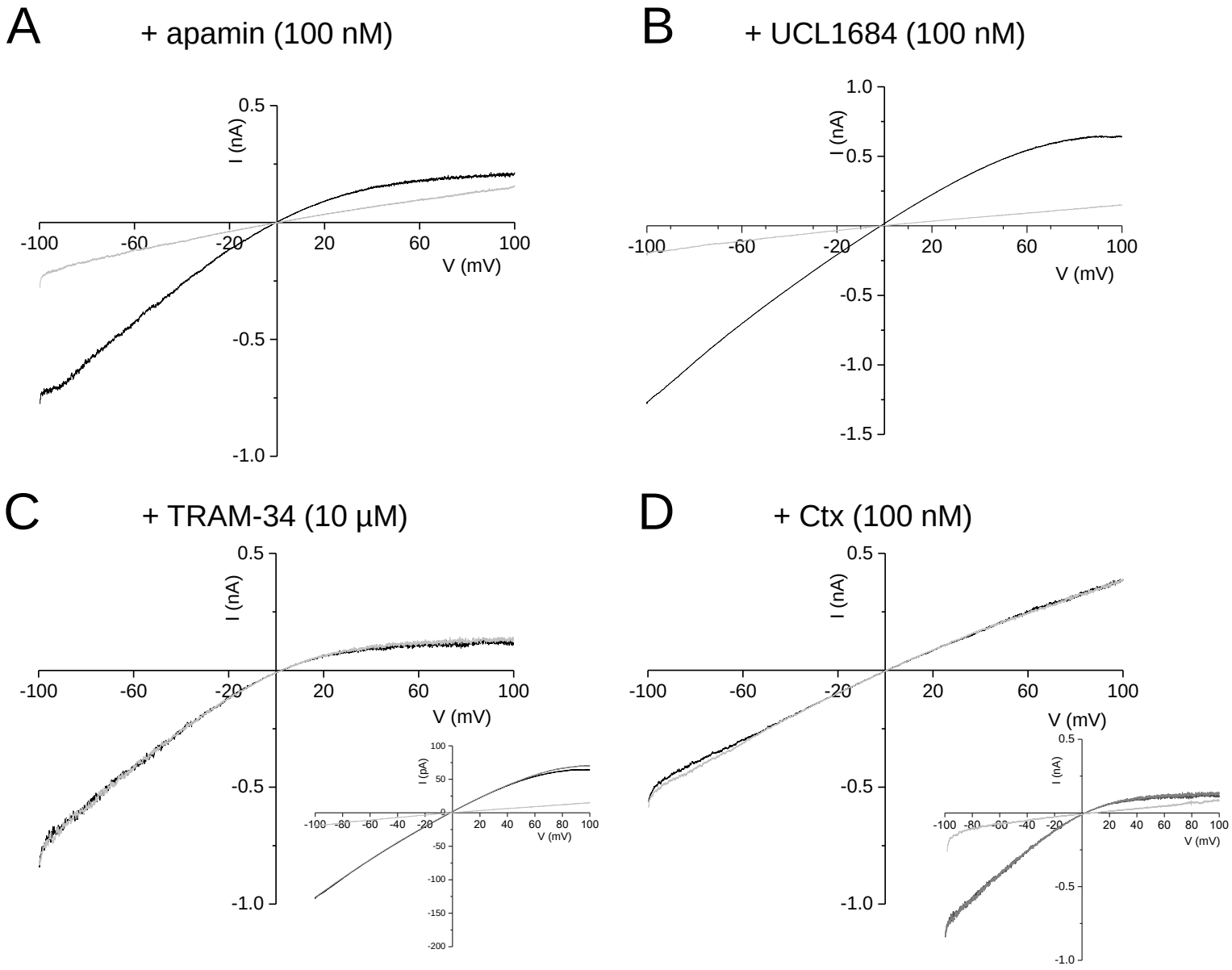
A
+ apamin (100 nM)
I (nA)
V (mV)
B
+ UCL1684 (100 nM)
I (nA)
V (mV)
C
+ TRAM-34 (10 µM)
I (nA)
V (mV)
I (pA)
V (mV)
D
+ Ctx (100 nM)
I (nA)
V (mV)
I (nA)
V (mV)

Figure 3

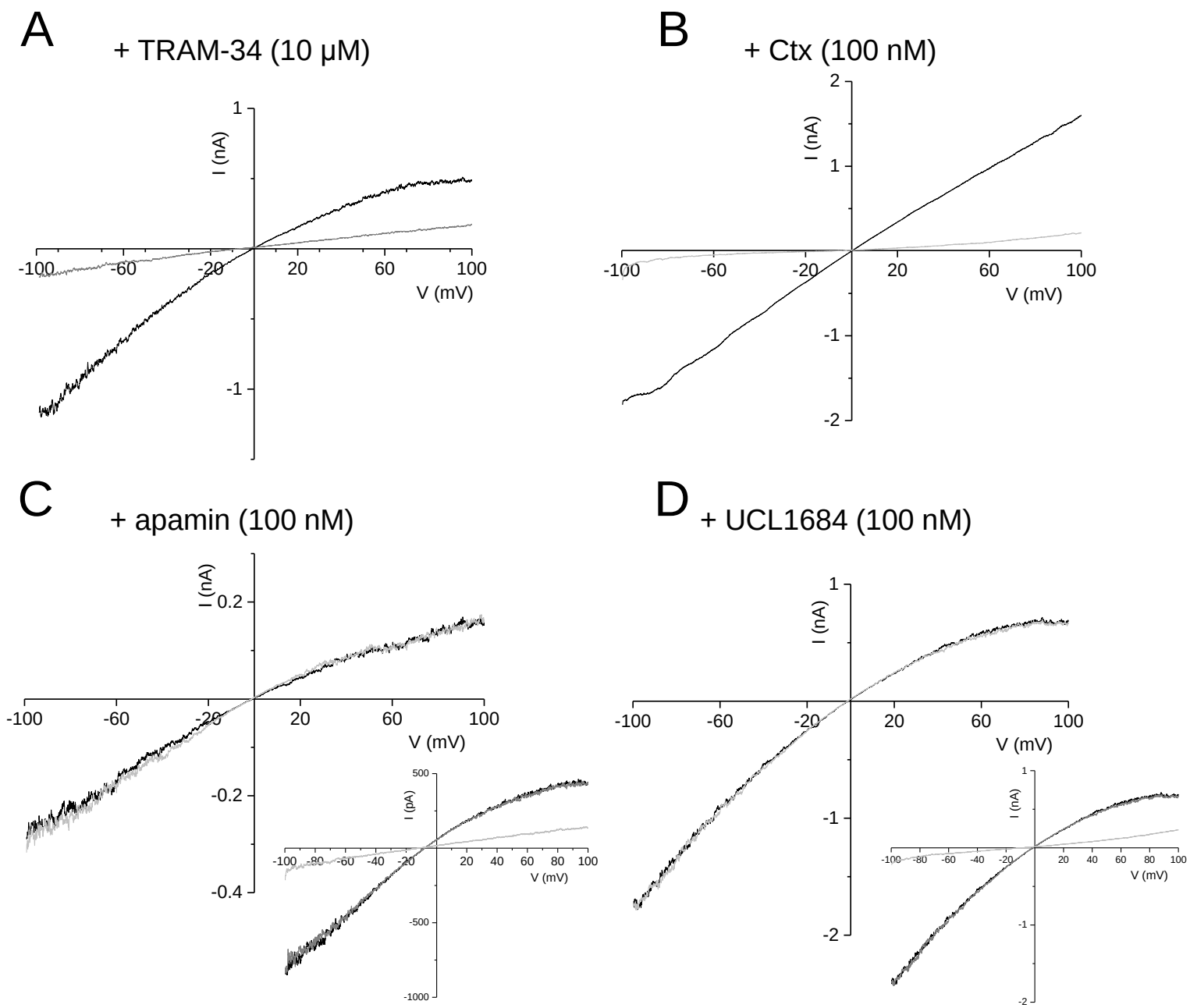
A
+ TRAM-34 (10 µM)
I (nA)
V (mV)
B
+ Ctx (100 nM)
I (nA)
V (mV)
C
+ apamin (100 nM)
I (nA)
V (mV)
I (pA)
V (mV)
D
+ UCL1684 (100 nM)
I (nA)
V (mV)
I (nA)
V (mV)

Figure 4

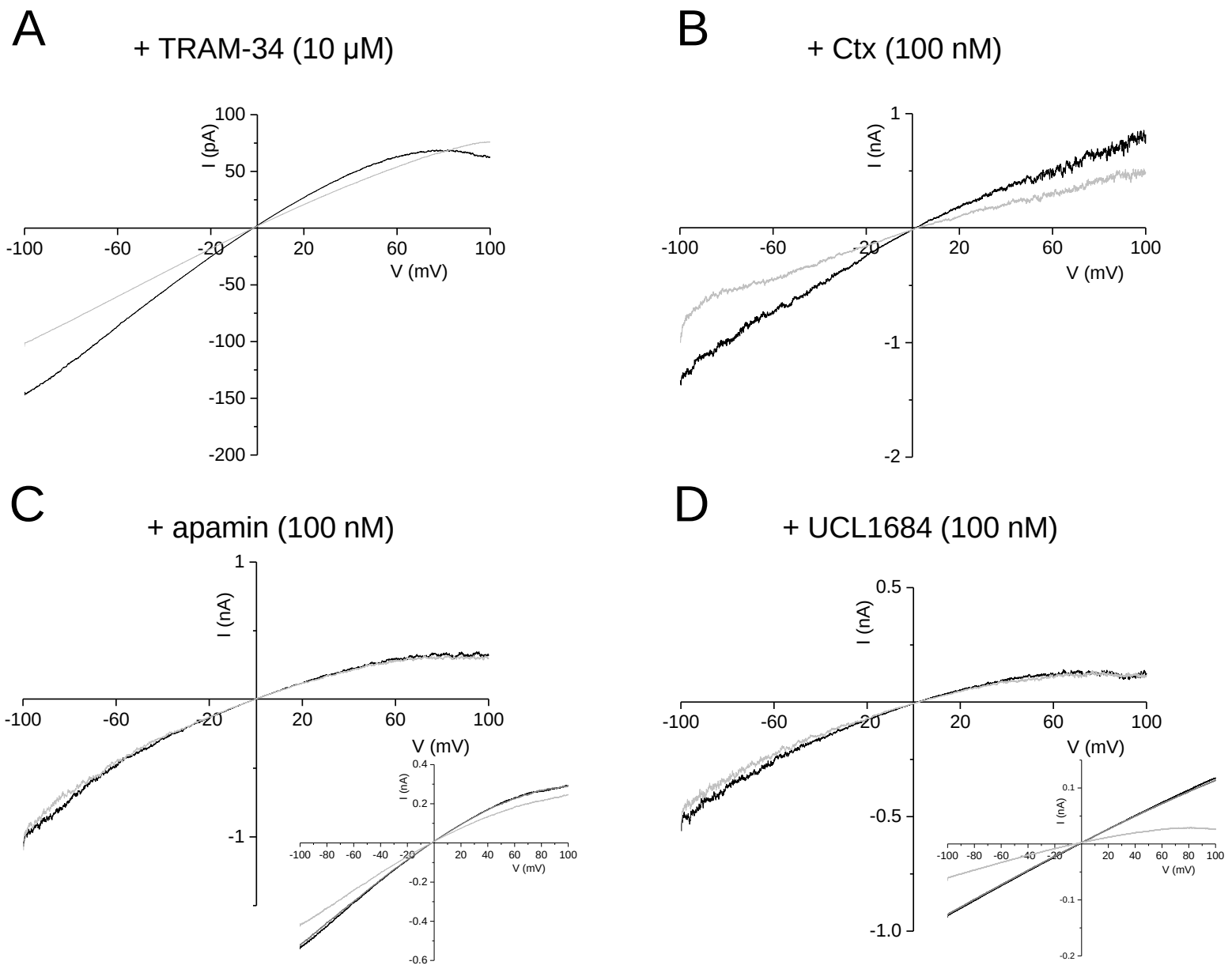
A
+ TRAM-34 (10 µM)
I (pA)
V (mV)
B
+ Ctx (100 nM)
I (nA)
V (mV)
C
+ apamin (100 nM)
I (nA)
V (mV)
D
+ UCL1684 (100 nM)
I (nA)
V (mV)

Figure 5

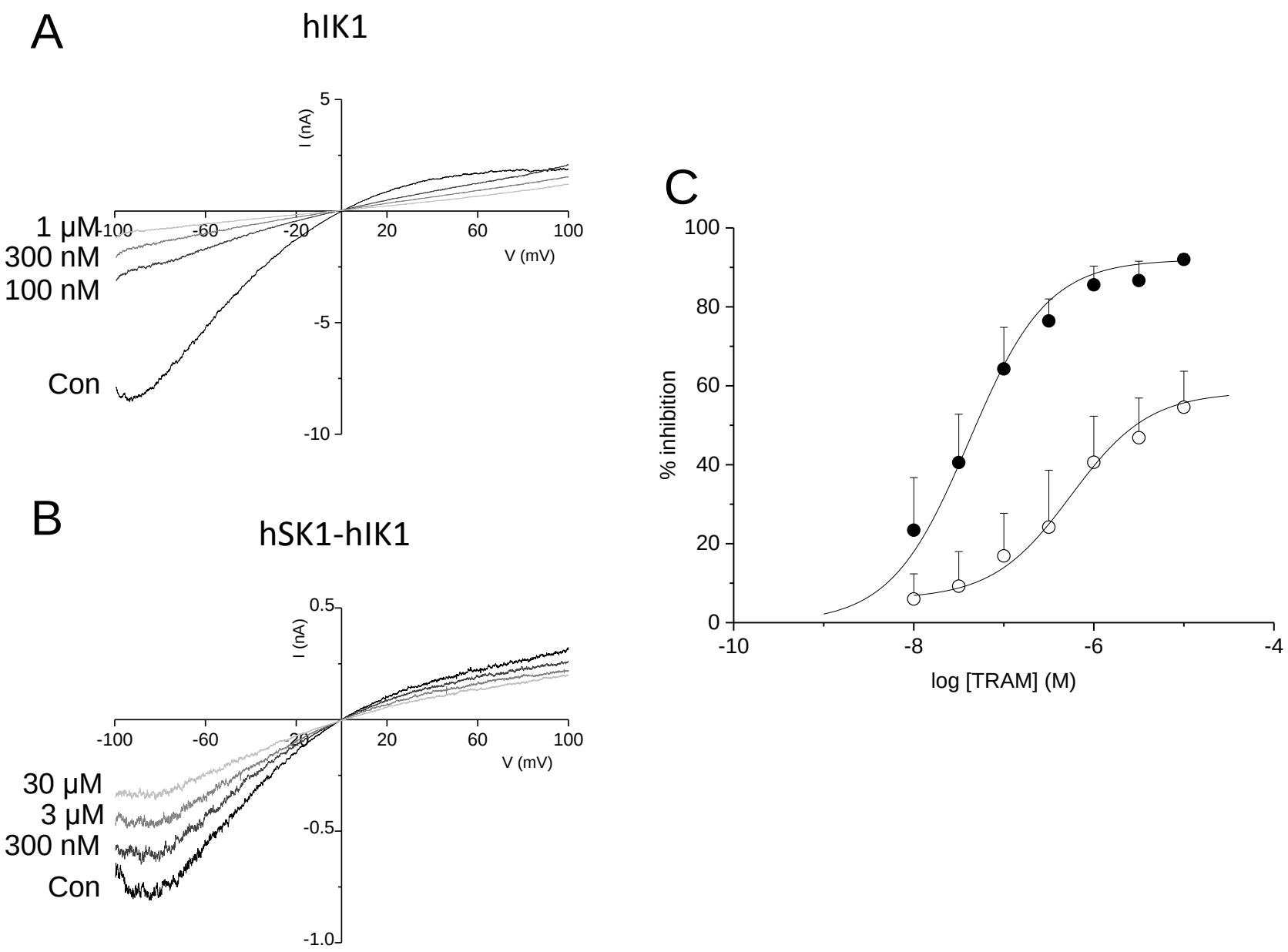
A
hIK1
I (nA)
5
-5
-10
-100
-60
-20
20
60
100
V (mV)
1 μM
300 nM
100 nM
Con
B
hSK1-hIK1
I (nA)
0.5
-0.5
-1.0
-100
-60
-20
20
60
100
V (mV)
30 μM
3 μM
300 nM
Con
C
% inhibition
100
80
60
40
20
0
-10
-8
-6
-4
log [TRAM] (M)

Figure 6

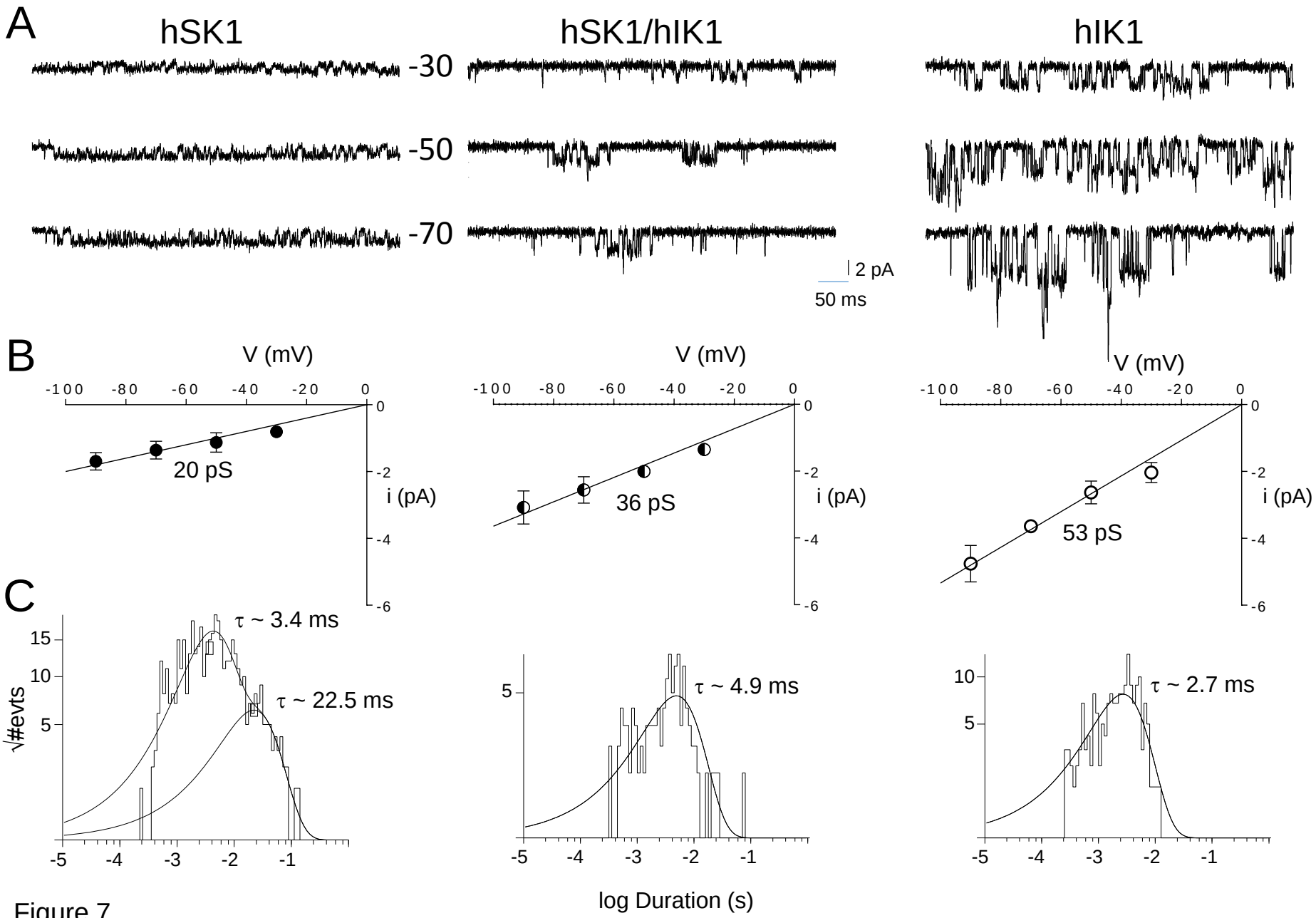
A
hSK1
hSK1/hIK1
hIK1
-30
-50
-70
2 pA
50 ms
B
V (mV)
-100 -80 -60 -40 -20 0
0 -2 -4 -6
i (pA)
20 pS
36 pS
53 pS
C
√#evts
τ ~ 3.4 ms
τ ~ 22.5 ms
τ ~ 4.9 ms
τ ~ 2.7 ms
-5 -4 -3 -2 -1
log Duration (s)

Figure 7